analytical chemistry

pubs.acs.org/ac Article

Trace Biomolecule Detection with Functionalized Janus Particles by Rotational Diffusion

Wei-Long Chen and Han-Sheng Chuang*

Cite This: https://dx.doi.org/10.1021/acs.analchem.0c01733 Read Online

ACCESS | Metrics & More | Article Recommendations | Supporting Information

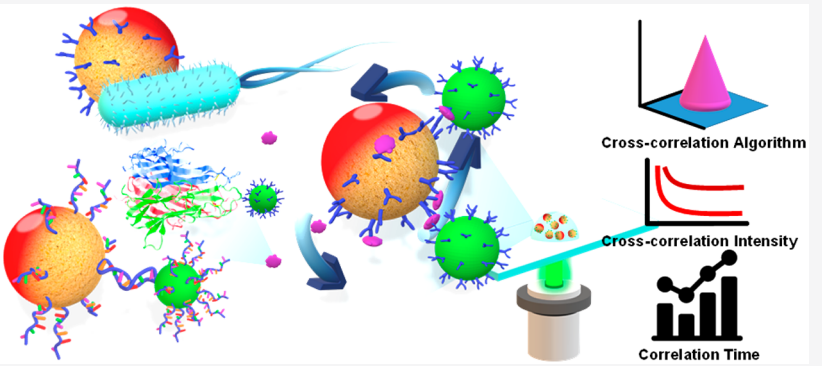

ABSTRACT: Cytokines are small proteins secreted by cells in innate and adaptive immune systems. Abnormal cytokine secretion is often regarded as an early cue of dysregulation of homeostasis due to diseases or infections. Early detection allows early medical intervention. In this study, a natural phenomenon called rotational Brownian motion was characterized by Janus particles and its potential use in detection of trace biomolecules explored. Through the functionalization of the Janus particles with an antibody, the target cytokine, that is, tumor necrosis factor-α, was measured in terms of rotational diffusion. Rotational diffusion is highly sensitive to the particle volume change according to the Stokes−Einstein−Debye relation and can be quantified by blinking signal. Accordingly, 1 μm half-gold and half-fluorescent microbeads were conjugated with 200 nm nanobeads through sandwiched immunocomplexes. The light source, lead time for stabilization, and purification were investigated for optimization. Particle images can be captured with green light at 5 Hz within 300 s. Under such conditions, the functionalized Janus particles eventually achieved a limit of detection of 1 pg/mL. The rotational diffusometry realized by Janus particles was power-free and feasible for ultrasensitive detection, such as early disease detection.

Cytokines are small proteins secreted by cells for cell signaling in innate and adaptive immune systems. The homeostatic levels of cytokines have been strongly associated with the health of our bodies.[1,2] For instance, tumor necrosis factors alpha (TNF-α), interleukins, and interferons are typically released in the bloodstream to regulate the immune system for exogenous invasions or endogenous abnormalities;[3] their presence can be a vital sign of certain infections or diseases. Although early detection allows early medical interventions in preventive medicine, low-abundant analytes pose a high barrier for modern sensing techniques.[4] To solve the problem, many research groups developed highly sensitive and precise devices. Takemura et al.[5] reported a technique that involved the use of gold/magnetic nanocomposite particles coupled with quantum dots for the detection of low norovirus concentration on the basis of localized surface plasmon resonance (SPR). Afterward, a two-step signal amplification of the prostate-specific antigen using two-sized gold nanoparticles and a consecutive signal amplification system was proposed by Zhang et al.[6] for prostate cancer. Paper-based immunoassays have emerged as an easy-to-use technique in many fields of detection. After the surface modification of paper by carboxymethyl cellulose, a previous study exhibited its highly sensitive and high-throughput potential in the measurement of tuberculosis diagnosis.[7] However, different from the methods mentioned above, diffusometry relies on a self-driving capability generated from random colloidal movement called Brownian motion. Therefore, diffusometry is free from power failure and is a sophisticated sample preprocessing method. According to the Stokes−Einstein relation, the translational diffusion of particles is inversely proportional to the particle diameter when the ambient temperature and the viscosity of fluid are controlled

Received: April 22, 2020
Accepted: September 15, 2020
Published: September 15, 2020

https://dx.doi.org/10.1021/acs.analchem.0c01733
Anal. Chem. XXXX, XXX, XXX−XXX

well.[8] Such conventional diffusometry has been developed in detecting microscale temperatures,[9] viscosities of various fluids,[10,11] and biological targets.[12,13] Despite the pioneering work done in these previous studies,[14,15] the limit of detection (LOD) is relatively restricted by the spatial resolution of a digital camera. The optimal LOD of translational diffusometry that has been achieved to date reaches nearly 10 pg/mL,[12] but this capability remains insufficient in several special applications, such as toxin detection,[16] diabetic retinopathy (DR), dry eye symptom,[17,18] or pathogens.[19,20] Rotational Brownian motion has drawn less public attention over the past decades because of difficulty in realization compared with translational Brownian motion. Nevertheless, rotational Brownian motion shows higher sensitivity than its translational counterpart to the particle volume change according to the Stokes−Einstein−Debye relation.[21] Therefore, rotational Brownian motion provides an effective alternative to advance the LOD, especially for trace biomolecules. Our previous study successfully investigated the microvolume viscosity of different oils on the basis of the rotational diffusometry.[22] However, this effective technique has not yet been characterized well for the detection of the trace small molecules. Hence, we developed a rotational diffusometry in the combination of functionalized Janus particles in detecting the presence of biomolecules. Several special particles, such as colloidal dimers, colloidal tetrahedral clusters, diamond nanoparticles, and Janus particles, have been used to reveal the signal of rotational Brownian motion.[23−26] Among the above-mentioned particles, Janus particles have been selected in this research because of their excellent surface scattering characteristics. For such Janus particles, several synthetic methods have been discussed in various papers.[27,28] The physical deposition reported by Casagrande et al.[29] in 1988 was favorably used in this study because of the ease of realization. In terms of the specific fabrication, a gold film was first coated on the half-side of 1 μm fluorescent polystyrene (PS) particles. The high biocompatibility of gold can facilitate the grafting of the subsequent biological complexes. Additional 200 nm PS beads were grafted to the Janus particles through sandwiched immunocomplexes in the presence of TNF-α to enhance the signal. Consecutive blinking images were captured at 5 Hz by a digital camera for 300 s. The cross-correlation algorithm was then applied to evaluate the degree of rotational diffusion by analyzing the consecutive particles images. Correlation time, which served as a quantitative index of the rotational Brownian motion, was obtained from the exponential curve fitting of the time-dependent correlation intensity.[10] The correlation time increased with the particle diameter because of reduced translational and rotational Brownian motion. Notably, this concept can be seen in another similar technique, termed differential dynamic microscopy (DDM),[26,30,31] that was originally developed for the collective dynamics of colloids. Therefore, DDM can also provide high-throughput measurements suitable for low-resolution microscopy with a large field of view. Several parameters, including light source, lead time for stabilization, and purification, were investigated to evaluate the efficiency of the Janus particle enabled diffusometry. The final result showed that the correlation time was sensitive to the increase in TNF-α concentration. Compared with the conventional enzyme-linked immunosorbent assay (ELISA) reader, this technique appeared to improve the LOD by nearly 1000-fold, thereby reaching 1 pg/mL. Overall, the Janus particle-enabled rotational diffusometry provides an insight into the detection of trace biomolecules and can be used in early disease diagnosis in the future.

MATERIALS AND METHODS

Materials. All of the PS particles were purchased from Thermo Fisher Scientific (Waltham, MA, U.S.A.). The mouse monoclonal anti-TNF-α immunoglobulin G (ab8348), TNF-α (ab9642), gold conjugation kit (ab154876), and rabbit polyclonal anti-TNF-α immunoglobulin G (ab9635) provided by Abcam were used to form sandwiched immunocomplexes. Bovine serum albumin (BSA) was purchased from Sigma-Aldrich (A2153, Sigma). The 1× phosphate-buffered saline (PBS) was diluted from 10× PBS (URPBS001, UniRegion Bio-Tech) with sterilized deionized water. PBST was prepared by mixing 1× PBS with 1% Tween 20 (P1379, Sigma).

Theoretical Relationship between Diffusivity and Particle Size. Brownian motion, including translational and rotational motion, is a random particle movement. According to the Stokes−Einstein equation,[8] translational Brownian motion can be expressed as eq 1, whereas rotational Brownian motion is defined by Stokes−Einstein−Debye equation, which is expressed as follows:[21]

$$D_t = \frac{k_B T}{3\pi\mu d_p} \tag{1}$$

$$D_r = \frac{k_B T}{\pi\mu d_p^{\,3}} \tag{2}$$

where k_B is the Boltzmann constant, T is the absolute temperature, μ is the viscosity of the liquid, d_p denotes the particle diameter, and D_t and D_r represent translational and rotational diffusion coefficients, respectively. According to eqs 1 and 2, the translational Brownian motion was inversely proportional to the particle diameter, whereas the rotational Brownian motion was inversely proportional to the cubic particle diameter under the same temperature and viscosity. The rotational Brownian motion is a formidable technique to detect the diameter of particles. To investigate the rotational Brownian motion, we used Janus particles to generate blinking signal. Instead of tracking single particles, the correlation intensity was calculated from the comparison of a series of particle images within a time interval Δt using the cross-correlation algorithm. The statistical analysis allowed compromised image quality but still achieved a result with more data, less effort, and high efficiency. The cross-correlation intensity was equivalent to the peak value of the cross-correlation function. The peak value decreased when the time interval increased. The intensity diagram was then normalized from the following exponential regression:[10]

$$A \exp\left(-\frac{t}{\phi}\right) + B \tag{3}$$

where A and B are constants, t represents the elapsed time, and ϕ denotes the correlation time of the intensity diagram. The correlation time can be expressed as follows:

$$\phi = \frac{\mu V}{k_B T} \tag{4}$$

where V indicates the volume of particle, which is proportional to correlation time when the viscosity of the liquid and temperature are fixed.

https://dx.doi.org/10.1021/acs.analchem.0c01733
Anal. Chem. XXXX, XXX, XXX−XXX

To verify the improvement in diffusivity resulting from rotational Brownian motion as compared with translational Brownian motion, an approximate model was constructed to simulate the diffusive behavior of an immunocomplexed Janus particle. Instead of building a complicated particle morphology, an equivalent volume diameter was first employed to represent the overall diameter increase of the immunocomplexed Janus particle, which can be formulated as

$$d_V = \left(\frac{6V}{\pi}\right)^{1/3} \quad (5)$$

where V is the new particle's volume, including the volume of a Janus particle and the total volume of conjugated PS particles. Next, the equivalent volume diameter can be substituted into the Stokes−Einstein−Debye relation to derive a decent diffusivity value of the Janus particle in a medium. For demonstration, the translational and rotational diffusivity changes with respect to the attached small PS particles are depicted in Figure S1 (simulation of translational and rotational Brownian motions for immunocomplexed particles). The rotational diffusion brings down the diffusivity faster than the translational diffusion. The simulation eventually provides a theoretical way to predict the relationship between the diffusivity and the concentration of attached small PS particles.

The orientational bias due to the gold coating was evaluated by the particle Péclet number (Pe_r),[32] which is defined as a ratio of gravitational energy to thermal energy (Supporting Information, formula of the Péclet number of rotational Brownian motion). For rotational diffusion, the equation is modified as

$$Pe_r = \frac{\dot{\gamma}}{D_r} = \frac{\frac{2}{3}\pi(R^3 - r^3)(\rho_g - \rho_l)gr_c}{k_B T} \quad (6)$$

where r_c is the centroid of the hemispheric gold shell, $\dot{\gamma}$ is the angular velocity of the Janus particle, R and r represent the outer and inner radii of the hemispheric gold shell, g is the gravitational acceleration, and ρ_g and ρ_l are densities of gold and liquid, respectively. Considering that the 1 μm Janus particles (without PS particles) are suspended in a water solution, the particle Péclet number for rotational diffusion is only 0.56, implying that the rotational diffusion is not seriously affected by the gravity. Our experimental observations for both 1 and 3 μm Janus particles also showed good agreement with the theoretical prediction. Since the blinking signal would gradually disappear if the heavy side on the Janus particle turned to dominant, the orientational bias appeared to be negligible in this study.

Experimental Setup. The rotational Brownian motion was used to detect the TNF-α antigen by the change in particle diameter. In the presence of TNF-α antigen, the functionalized Janus and PS particles would form sandwiched immunocomplexes to change the particle diameter. Hence, 2 μL of the sandwiched immunocomplex suspension was pipetted on the glass slide. A glass cover was then placed on the top of the droplet with a spacer of approximately 155 μm. The rotational Brownian motion was observed under a fluorescence microscope (IX71, Olympus, Japan) with a 40× oil objective lens. The image sequences were captured by a charge-coupled device (CCD) (FL3-U3-13S2C-CS, Point Gray) and C-mount camera adapter (U-TV0.63XC, Olympus) with the resolution of 1280 pixels ×960 pixels (Figure 1). The blinking signal from the Janus particles was then analyzed by the cross-correlation algorithm, and then estimated a correlation time using the MATLAB software.

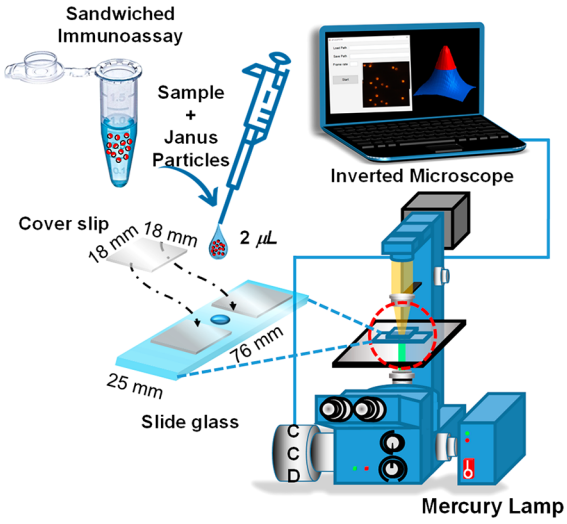

Figure 1. Scheme of the experimental setup. A total of 2 μL of the sample suspension was pipetted on the glass slide. The 40× objective lens was used to observed the Janus particles under a IX71 microscope. The images captured by the CCD were then calculated in MATLAB software.

Janus Particles Fabrication. To prepare uniformly dispersed Janus particles, we followed the procedure of physical deposition to make the Janus particles.[33,34] The PS particles were purchased from Thermo Fisher Scientific (Waltham, MA, U.S.A.). The size distribution of the 1 μm particles was defined by dynamic light scatting (Beckman Coulter). First, the glass slide was treated with oxygen plasma or a UV light (wavelength: 172 nm, Hamamatsu Flat Excimer, EX-mini) to prepare a hydrophilic surface. Second, the particle suspension was diluted to 0.1% solid in the solution of the surfactant Tween 20/ethanol (1:400 by volume).[35] Third, 100 μL of the diluted suspension was placed on the hydrophilic surface of the glass slide. The monolayer particles were formed on the glass slide after drying out the suspension. The thin layer of the gold film with 30 nm was deposited on the monolayer particles by an e-beam evaporator, with the coating rate 1 Å/s. The Janus particles were harvested from the glass slide though sonication for 3 h and transferred to the water solution with 1% (v/v) Tween 20. The Janus particles suspension was purified by two filter disks (pore sizes: 5.0 and 0.8 μm) to remove the aggregated particles or gold fragments. Finally, the suspension was concentrated to 2×10^9 particles/mL by centrifugation. The final suspension was stored at 4 °C for later surface modifications.

Antibody-Conjugated Janus Particles. The mouse monoclonal anti-TNF-α IgG was covalently attached on the gold side of the Janus particles by a gold conjugation kit. The reagents were stored at −20 °C. The stock antibodies were diluted to 0.5 mg/mL by the gold antibody diluent. Diluted antibodies (12 μL) were mixed with 42 μL of gold reaction buffer in a 1.5 mL microfuge tube. The mixture (45 μL) was then incubated with 20 μL of the Janus particle suspension in a shaker (400 rpm) at room temperature for 15 min. Then, the mixture was mixed gently with 5 μL of the gold quencher buffer, and the functionalized Janus particle suspension with a final volume of 70 μL was stored at 4 °C overnight. The unbound antibodies

https://dx.doi.org/10.1021/acs.analchem.0c01733
Anal. Chem. XXXX, XXX, XXX−XXX

were washed out and transferred to PBST solution by centrifugation at 13 500 rpm thrice.

Antibody-Conjugated PS Particles. In general, a high concentration of small particles increases the chance of aggregation, whereas a low concentration of small particles lowers the reaction efficiency. To estimate the appropriate concentration of small particles to be used, the total gold surface area of the large Janus particles was first calculated. Under the ideal assumption of being fully covered by antibodies (12 nm × 12 nm), the maximum number of 200 nm PS particles was around 39 with the gold surface area of a single Janus particle being 1.57×10^{-12} m^2 and the projected area of a single PS particle being 4×10^{-14} m^2.

The rabbit polyclonal anti-TNF-α IgG was coupled to the 200 nm amine-modified PS particles (F8764, Thermo Fisher) via covalent linkage. A total of 6 μL of the particle solution (4.54×10^{12} particles/mL) was washed with 200 μL of 50 mM 2-(*N*-morpholino)ethanesulfonic acid buffer (MES buffer; pH of 5.5, M3671, Sigma) at 13 500 rpm for 6 min for three cycles. Then, the suspension was sonicated to prevent aggregation. To activate the carboxyl group on the antibody, we mixed 10 μL of 0.5 mg/mL polyclonal antibody, 6 μL of 10 mg/mL 1-ethyl-3-(3-(dimethylamino)propyl)-carbodiimide, 12 μL of 10 mg/mL *N*-hydroxysuccinimide, and 30 μL of the MES buffer in the tube, and then incubated the mixture in a shaker at 25 °C and 800 rpm for 15 min. The mixture was incubated with particle suspension at 4 °C and 800 rpm for 4 h in the shaker. The mixture was vortexed every 1 h to prevent aggregation. After storing at 4 °C overnight, the unbound antibodies were washed away from the suspension three times with PBST by centrifugation at 13 500 rpm.

Sandwiched Immunocomplexes. The functionalized Janus particle suspension (20 μL) was first incubated in a shaker with 10 μL of different concentrations (1 pg/mL to 100 μg/mL) of TNF-α at room temperature and 800 rpm for 1 h, followed by three washing cycles to remove unbound antigens. Notably, this washing step was intentionally implemented here to prevent later random aggregation induced by the free suspended antigens. The calibrated concentrations of antigens (1 pg/mL to 100 μg/mL) were lower than those of both capture and probe antibodies to reduce free suspended antigens. For the interference group, 10 μL of PBST and 0.1% BSA were added to be incubated with functionalized Janus particle suspension. Then, 10 μL of the functionalized PS particle suspension was added to the solution at 25 °C and 800 rpm for 1 h. Antigens and antibodies are usually too small to induce diffusivity changes and electrochemically stable in the solutions. Therefore, 200 nm PS particles were required to enhance the volume change in the presence of target antigens. The final sandwiched immunocomplexes were formed after the incubation.

RESULTS AND DISCUSSION

Realization of Quantitative Rotational Brownian Motion. To quantify rotational Brownian motion, we used the Janus particles here to produce blinking signal. To fabricate the Janus particles (Figure 2A), we made glass slides superhydrophilic by exposing them to an excimer lamp (172 nm, Hamamatsu Flat Excimer, EX-mini). Next, 1 μm fluorescent PS particles were deposited on the glass slides to form a monolayer and then covered with a 30 nm gold film by e-beam evaporation. Afterward, the gold-coated particles were collected by sonicating the glass slides in a 50 mL centrifuge tube for 3 h. Finally, the colloidal suspension was injected through a filter

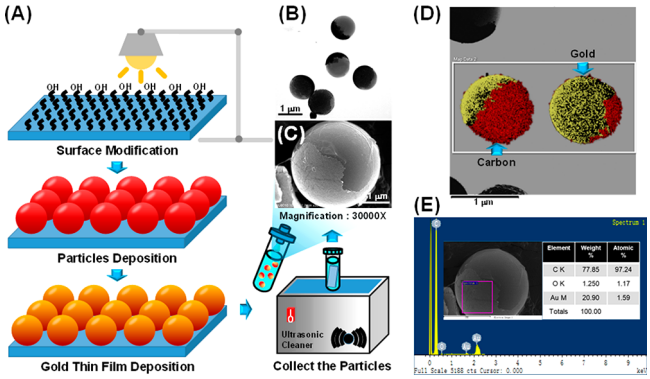

Figure 2. Janus particle fabrication. (A) The glass slide substrate was treated by oxygen plasma or a specific wavelength of UV light to increase hydrophilicity. Then, a 200 μL drop of fluorescent PS particle suspension was deposited on the surface of the glass slide. The monolayer PS particles were formed by drop-coating. A gold thin film was deposited on the monolayer PS particles to form the Janus particles by an e-beam evaporator. Finally, the Janus particles were collected by an ultrasonic cleaner and purified by a filtering process. (B) TEM image of the 1 μm Janus particles. (C) SEM image of the 3 μm Janus particles. (D) Elemental analysis of the 1 μm Janus particles by TEM; red dots indicate C, whereas yellow dots denote Au. (E) Elemental composition of the 3 μm Janus particles by SEM.

paper with 5 μm pore size to remove large gold fragments or particle aggregates. Then, it was passed through another filter paper with 0.8 μm pore size to separate tiny contaminants. The right-sized Janus particles (1 μm) can be eventually collected from the second filter paper by washing it with the PBS buffer solution. Liquid transmission electron microscopy (TEM) and scanning electron microscopy (SEM) were used to examine the surface morphology of the Janus particles and their compositions. One side of the Janus particles was covered with a gold film as designed, whereas the other side remained uncovered (Figure 2, parts B and C). Irregular edges were formed on the gold coating. These irregular edges primarily resulted from trimming action during sonication. Given that the computation algorithm was based on the blinking signal, the final analysis was not altered by the imperfection. A reconstructed particle model synthesized by energy-dispersive spectroscopy (JEM-2100F, JEOL) reflected the surface distribution of the elements on the particle (Figure 2D). The pseudocolors indicated that the purified Janus particle was in good agreement with the desired gold coating. The composition of the elements measured on the surface is also depicted in Figure 2E.

The correlation intensity was determined from two consecutive blinking images by the cross-correlation algorithm. Translational diffusion, rotational diffusion, out-of-plane particles, and out-of-focus particles all resulted in some loss in the correlation intensity. Given 1 μm particles in a water solution, the particle Péclet numbers for plain PS and Janus particles were estimated to be 0.15 (referred to the literature[30,32]) and 0.56 (derived from eq 6), respectively. According to the definition of the particle Péclet number, the low *Pe* hence implies the translational diffusion and rotational diffusion to be the dominant factors of the correlation intensity for plain PS and Janus particles, respectively, in this study (tracking of PS particles and Janus particles, Figure S2). The correlation between a pair of blinking particle images with an increased time interval from 0 to 300 s was calculated. In the calculation, the first particle image was fixed at 0 s but the second image was

https://dx.doi.org/10.1021/acs.analchem.0c01733
Anal. Chem. XXXX, XXX, XXX−XXX

shifted by 0 + Δt s. The relationship between the correlation intensity and the time (Δt) was then plotted as an intensity diagram (Figure 3A). The correlation intensity appeared to

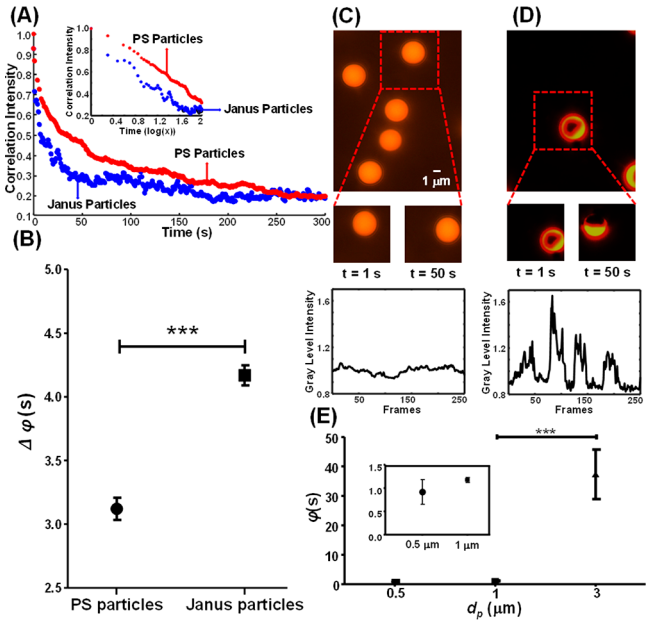

Figure 3. Janus particles against PS particles. (A) Cross-correlation intensity decreases with time. The red and blue curves refer to PS and Janus particles, respectively. The inset exhibits a close-up semilog plot of the first 100 s. (B) Correlation time differences of the PS and Janus particles. (C) The tracking system used to evaluate the gray-level intensity of the PS particles. (D) The tracking system used to evaluate the gray-level intensity of Janus particles. (E) Size effect of the Janus particles; the inset shows the correlation times of the 0.5 and 1.0 μm Janus particles.

decline with the elapsed time because of loss of pairs. Strong diffusion rapidly brought down the correlation intensity, whereas weak diffusion showed a slow decline in the correlation intensity. Moreover, Janus particle images containing both rotational and translational Brownian motions appeared to impair the correlation intensity faster than their PS counterpart as well. Notably, the derived correlation function is composed of convolution (R_C), fluctuating noise component of the correlation estimator (R_F), and correlation between particles (R_D).[36] Unless R_C and R_F are removed, the actual correlation intensity will never drop to zero even though R_D is completely eliminated. An exponential trend, called correlation time, was derived from the curve fitting of the correlation intensity data along time to represent the quantitative declining speed. In principle, a fast-declining correlation intensity yielded a small correlation time and vice versa. To verify the improvement made from translational to rotational Brownian motion, we measured 1 μm Janus particles and 1 μm fluorescent PS particles with the same epifluorescence microscopy with a 40× objective. The evaluation was performed in terms of the correlation time (Figure 3B). The Δ correlation time ($\Delta\varphi$) indicates the correlation time differences between immunocomplexed and plain particles. A large $\Delta\varphi$ means high sensitivity. Rotational Brownian motion (measured from Janus particles) showed a higher correlation time change than its translational counterpart (measured from fluorescent PS particles). The blinking effect was also explicitly observed on Janus particles rather than the fluorescent PS particles, thereby indicating the necessity of Janus particles in the study of the rotational Brownian motion. Janus particles exhibited rotational and translational diffusion. The translational diffusion was mitigated by reducing particle diameter and camera resolution. The translational diffusion can be observed by using the fluorescent PS particles (Figure 3C), whereas the rotational diffusion can be only observed by using the Janus particles (Figure 3D; comparison of PS and Janus particles in the fluorescence images, Video S1; tracking of PS particles and Janus particles, Figure S2). Three different particle diameters, namely, 0.5, 1.0, and 3.0 μm, were investigated for their feasibility in the study (Figure 3E). The correlation times for 0.5, 1.0, and 3.0 μm Janus particles were 0.90 ± 0.26, 1.17 ± 0.05, and 37.31 ± 3.77 s, respectively (dynamic changes of cross-correlation function, Video S2). As predicted, a small particle diameter resulted in a short correlation time, thereby indicating a large dynamic range of measurement and high sensitivity. However, the differences in the correlation times between 1.0 and 0.5 μm Janus particles were not significant. This unexpected discrepancy was likely due to the fact that small particles tended to stack up instead of forming a monolayer during drying on a glass slide. The multilayer therefore resulted in the formation of additional particle aggregates, which disturbed the desired particle diameter. The ratio of the correlation time of the 1 μm Janus particles to that of 3 μm Janus particles was 31.89, which was slightly larger than the predicted number, that is, 27, which was derived from eq 4. The deviation indicated that the data measured from Janus particles was likely a combination of the rotational and translational Brownian motions. Nevertheless, the rotational Brownian motion retained the dominant factor that contributed to the computation of the final correlation time according to the comparison shown in Figure 3B. Considering all the above-mentioned conjectures, the 1 μm Janus particles were eventually selected for the realization of the rotational diffusometry in this study.

Characterizations of Rotational Brownian Motion. In addition to Janus particles, several other factors also seemed to alter the quality of measurement. For optimization, three major factors, light source, lead time for signal stabilization, and purification, were herein investigated. Prior studies[37,38] stated that gold showed strong SPR behavior as irradiated by a light source at its absorption peak (520−550 nm). To examine the SPR effect, we generated two light colors (Figure 4A), namely, green and blue, from two optical filters (530−550 and 460−495 nm) in the epifluorescence microscope (IX71, Olympus), and these were used to excite Janus particles.[39] The correlation time decreased as the Janus particles were irradiated by green light. Given that a short correlation time indicates strong diffusion, SPR can be used to improve the LOD through enhanced rotational Brownian motion. For the bulk temperature increase due to SPR, a slight temperature increase of around 3.9 °C was measured in the medium under the green irradiance of 2.2×10^4 W/m^2 (notice: the irradiance was measured right next to the objective lens) by using a temperature-dependent dye, rhodamine B (evaluation of temperature increase due to SPR, Figure S3). The measurement was conducted by following the past studies.[3,4] Although the local temperature could not be precisely measured in our current setup, the temperature on AuNPs appeared to be higher than the bulk temperature. Considering that no significant dissociation was observed in our immunocomplexes, the local temperature could be assumed to be below 40 °C (notice: proteins become unstable above 40 °C). A similar setup in our past study[5] also showed no declining diffusivity

https://dx.doi.org/10.1021/acs.analchem.0c01733
Anal. Chem. XXXX, XXX, XXX−XXX

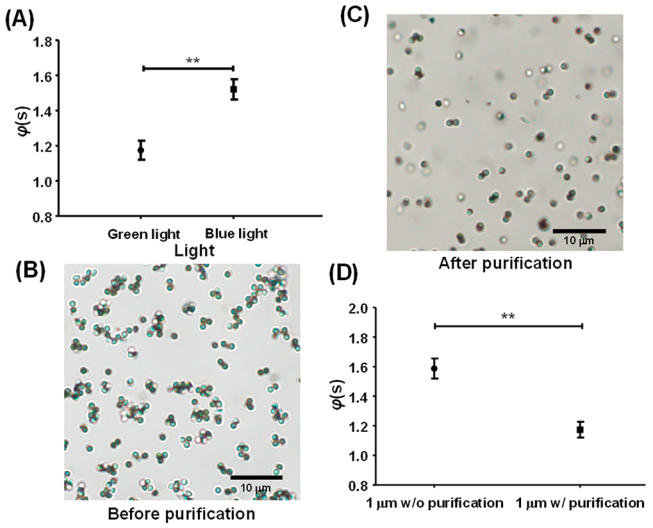

Figure 4. Evaluation of capture light source and purification. (A) The correlation times of green and blue light sources. (B and C) The images of the Janus particles with and without purification under microscopy. (D) The correlation time of the Janus particles with and without purification.

during measurement, implying no significant dissociation occurred. Given that the local temperature was likely to increase from 25 to 40 °C for the worst case and the local medium viscosity accordingly changed from 0.89 mPa·s to 0.65 mPa·s, the diffusivity in our system was estimated to increase by 44% under the SPR effect.

The size-dependent lead time needs to be investigated well to ensure that a correlation curve is completely rendered. Hence, 1 and 3 μm Janus particle were evaluated. The lead time is defined as the time frame required for the correlation intensity to reach stabilization. Given that the blinking frequency increased with reduced particle diameter, the correlation intensity declined faster for small particles than large particles, thereby resulting in different lead times for different particle sizes (determination of lead time for a stable correlation time, Figure S4). As expected, small particles required a short lead time for stabilization because of the relatively vigorous Brownian motion. This result suggested that the lead times for the 1 and 3 μm Janus particles were 25 and 110 s, respectively.

A colloidal suspension after sonication was generally mixed with numerous contaminants. A purification process with two-step filtering through the use of filter papers with pore sizes of 5.0 and 0.8 μm was performed (Figure 4, parts B and C). The Janus particles with purification appeared to yield a shorter correlation time than those without purification (Figure 4D). The long correlation time in the Janus particle without purification was attributed to the presence of particle aggregates or large gold fragments. The suspended fragmental gold films may also inhibit the formation of the immunocomplexes. Taking the mentioned concerns into consideration, the purified Janus particles were required for all experiments.

Detection of Trace Biomolecules with Janus Particles. The proposed technique was eventually applied for the detection of TNF-α, which is a distinct biomarker in the tear of patients with DR.[40] In this measurement, the 1 μm Janus particles were conjugated with anti-TNF-α IgG and then separately incubated with a wide range of concentrations of TNF-α (1 pg/mL to 10 μg/mL). Subsequently, the 200 nm PS particles conjugated with TNF-α probe antibody were mixed with the surface-modified Janus particles to form sandwiched immunocomplexes. The final sandwiched configuration that was composed of a Janus particle, immunocomplexes, and PS particles was then examined by TEM (Figure 5A). At the same

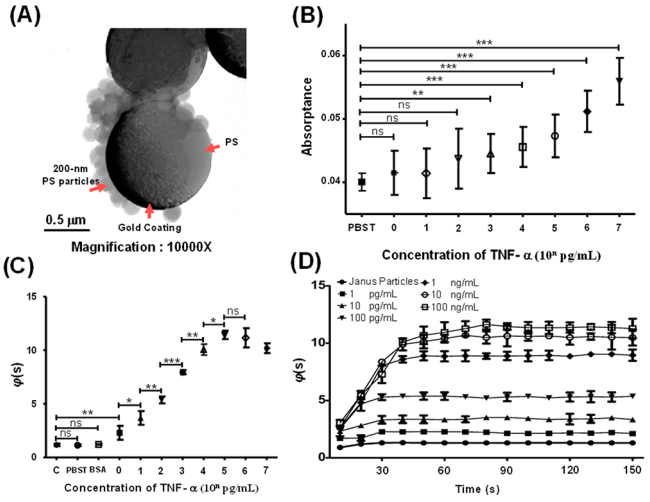

Figure 5. Comparison with the ELISA reader and the rotational Brownian motion-based immune sensor. (A) TEM image demonstrating that the antibodies were conjugated with the gold side of the Janus particles. (B) Different TNF-α concentrations detected by the ELISA reader. (C) Different TNF-α concentrations detected by the immune sensor (C: control). (D) The stabilization time of different TNF-α concentrations.

time, each concentration was also examined by ELISA for verification. In terms of rotational diffusion measurement, the experimental temperature of all microchips was maintained at 25 °C. Each sample was equally divided into six 2 μL colloidal droplets. The six droplets were placed on a microchip with a distance of 200 μm apart. A total of 60 s of blinking particle images were recorded for each concentration. The signal readouts of ELISA absorption and correlation time showed monotonic escalation with the increased concentration (Figure 5, parts B and C). The good agreement between the ELISA and our measurement validated the feasibility of the rotational diffusometry. The rotational diffusometry considerably achieved a lower LOD (1 pg/mL) and a higher resolution than conventional ELISA. The correlation time slightly decreased after the TNF-α concentration exceeded 100 ng/mL. This discrepancy may be attributed to the hook effect, which was caused by the competing immunoreactions from the free suspended antigens in the medium. The LOD was defined as the intersection of the three standard deviations of the control and trend line of the concentration. The 0.1% BSA and PBS with Tween 20 (PBST) were used herein to evaluate the specificity and interferences from the background. None of the BSA and PBST groups induced either interferences or nonspecific binding. Although the diffusivity change was mainly induced by the small PS particles, a recalibration will be required when the immunoassay is replaced with other binding mechanisms, such as aptamers, because the affinity, specificity, and kinetics of molecules are all different.

Given that large particles tended to increase the lead time for signal stabilization (determination of lead time for a stable correlation time, Figure S4), the same effect was observed in the Janus particles mixed with increased target biomolecules (Figure 5D). The required lead time for 100 ng/mL TNF-α to reach the

https://dx.doi.org/10.1021/acs.analchem.0c01733
Anal. Chem. XXXX, XXX, XXX−XXX

signal plateau was approximately 60 s. Nevertheless, the maximum lead time remained in the measurable range. This evaluation suggested that the Janus particles enabled rotational diffusometry, which can be a potential diagnostic tool in detecting various trace biomarkers of diseases at the early stage.

CONCLUSIONS

Abnormal cytokine secretion can be an effective biomarker for the dysregulation of homeostasis resulting from disease or infection. However, the detection of low-abundant biomarkers during the early stage remains a challenging task. This study presents a unique solution to achieve ultrasensitive detection of the trace biomolecules with the functionalized Janus particles on the basis of the rotational Brownian motion. Through physical deposition, the Janus particles were fabricated by coating a gold film on the half-side of fluorescent PS particles. After conjugating the Janus particles with a specific antibody, they will serve as smart probes to capture target analytes in a sample fluid. The 200 nm plain PS particles were conjugated with the immunocomplexed Janus particles to form a sandwiched configuration in enhancing the Brownian motion. The rotational Brownian motion was expressed in terms of blinking signal. As a result, the time-dependent cross-correlation of the consecutive images decreased rapidly with the increased concentration of analytes because of the increased volume of the Janus particles. The correlation time was obtained by fitting the time-dependent correlation intensity with an exponential curve. The characterizations of the Janus particles yielded three optimal parameters for rotational diffusometry. The final light color, lead time for signal stabilization, and purification were green light, 60 s, and purified 1 μm Janus particles, respectively. The calibrations of biomolecules, that is, TNF-α, between ELISA and rotational diffusometry were in good agreement, but the latter can even reach the LOD level of nearly 1 pg/mL. The developed rotational diffusometry can provide a valuable diagnostic for the urgent needs in ultrasensitive detection of trace biomolecules at the early stage of the diseases.

ASSOCIATED CONTENT

Supporting Information

The Supporting Information is available free of charge at https://pubs.acs.org/doi/10.1021/acs.analchem.0c01733.

Simulation of translational and rotational Brownian motions for immunocomplexed particles, tracking of PS particle and Janus particle, evaluation of temperature increase due to SPR, and determination of lead time for a stable correlation time (PDF)

Comparison of PS and Janus particles in the fluorescence images (MP4)

Dynamic changes of cross-correlation function (MP4)

AUTHOR INFORMATION

Corresponding Author

Han-Sheng Chuang − *Department of Biomedical Engineering and Center for Micro/Nano Science and Technology, National Cheng Kung University, Tainan 701, Taiwan;* orcid.org/0000-0002-7257-6565; Email: oswaldchuang@mail.ncku.edu.tw

Author

Wei-Long Chen − *Department of Biomedical Engineering, National Cheng Kung University, Tainan 701, Taiwan*

Complete contact information is available at: https://pubs.acs.org/10.1021/acs.analchem.0c01733

Author Contributions

The manuscript was written through contributions of all authors. All authors have given approval to the final version of the manuscript.

Notes

The authors declare no competing financial interest.

ACKNOWLEDGMENTS

This research was supported by the Ministry of Science and Technology under the Grants 107-2221-E-006-054-MY3 and 108-2628-E-006-002-MY3.

REFERENCES

(1) David, J. R. *Proc. Natl. Acad. Sci. U. S. A.* **1966**, *56* (1), 72−77.
(2) Cohen, S.; Bigazzi, P. E.; Yoshida, T. *Cell. Immunol.* **1974**, *12* (1), 150−159.
(3) Boyle, J. J. *Curr. Vasc. Pharmacol.* **2005**, *3* (1), 63−68.
(4) Poste, G. *Nature* **2011**, *469* (7329), 156−157.
(5) Takemura, K.; Lee, J.; Suzuki, T.; Hara, T.; Abe, F.; Park, E. Y. *Sens. Actuators, B* **2019**, *296*, 126672.
(6) Zhang, P. J.; Yang, J.; Liu, D. B. *Electrophoresis* **2019**, *40* (16−17), 2211−2217.
(7) Yang, C. H.; Chen, C. A.; Chen, C. F. *Sens. Actuators, B* **2018**, *265*, 506−513.
(8) Miller, C. C. *Proc. R. Soc. Lond. A* **1924**, *106* (740), 724−749.
(9) Mayor, P.; D'Anna, G.; Barrat, A.; Loreto, V. *New J. Phys.* **2005**, *7*, 28.
(10) Lavalette, D.; Tetreau, C.; Tourbez, M.; Blouquit, Y. *Biophys. J.* **1999**, *76* (5), 2744−2751.
(11) Gabbasov, R.; Yurenya, A.; Nikitin, A.; Cherepanov, V.; Polikarpov, M.; Chuev, M.; Majouga, A.; Panchenko, V. *J. Magn. Magn. Mater.* **2019**, *475*, 146−151.
(12) Chuang, H. S.; Chen, Y. J.; Cheng, H. P. *Biosens. Bioelectron.* **2018**, *101*, 75−83.
(13) Wang, J. C.; Chi, S. W.; Shieh, D. B.; Chuang, H. S. *Sens. Actuators, B* **2019**, *278*, 140−146.
(14) Ueda, H.; Tsumoto, K.; Kubota, K.; Suzuki, E.; Nagamune, T.; Nishimura, H.; Schueler, P. A.; Winter, G.; Kumagai, I.; Mahoney, W. C. *Nat. Biotechnol.* **1996**, *14* (13), 1714−1718.
(15) Wang, R. G.; Zhang, W.; Wang, P. L.; Su, X. O. *Microchim. Acta* **2018**, *185* (3), 191.
(16) Cheng, H. P.; Chuang, H. S. *Acs Sensors* **2019**, *4* (7), 1754−1760.
(17) Park, Y. G.; Roh, Y. J. *J. Diabetes Res.* **2016**, *2016*, 1753584.
(18) Stefansson, E.; Bek, T.; Porta, M.; Larsen, N.; Kristinsson, J. K.; Agardh, E. *Acta Ophthalmol. Scand.* **2000**, *78* (4), 374−385.
(19) Wang, J. C.; Tung, Y. C.; Ichiki, K.; Sakamoto, H.; Yang, T. H.; Suye, S.; Chuang, H. S. *Biosens. Bioelectron.* **2020**, *148*, 111817.
(20) Wang, J. C.; Chi, S. W.; Yang, T. H.; Chuang, H. S. *Acs Sensors* **2018**, *3* (10), 2182−2190.
(21) Debye, P. *Polar Molecules*; Chemical Catalog Company, Inc.: New York, 1929 *J. Soc. Chem. Ind., London* **1929**, *48* (43), 1036−1037.
(22) Chen, C. J.; Chen, W. L.; Phong, P. H.; Chuang, H. S. *Sensors* **2019**, *19* (5), 1217.
(23) Wang, P. Y.; Mason, T. G. *Phys. Chem. Chem. Phys.* **2017**, *19* (10), 7167−7175.
(24) Hunter, G. L.; Edmond, K. V.; Elsesser, M. T.; Weeks, E. R. *Opt. Express* **2011**, *19* (18), 17189−17202.
(25) Fujiwara, M.; Shikano, Y.; Tsukahara, R.; Shikata, S.; Hashimoto, H. *Sci. Rep.* **2018**, *8*, 14773.
(26) Wittmeier, A.; Holterhoff, A. L.; Johnson, J.; Gibbs, J. G. *Langmuir* **2015**, *31* (38), 10402−10410.
(27) Walther, A.; Muller, A. H. E. *Chem. Rev.* **2013**, *113* (7), 5194−5261.

(28) Zhang, J.; Grzybowski, B. A.; Granick, S. *Langmuir* **2017**, *33* (28), 6964−6977.
(29) Casagrande, C.; Veyssie, M. *C. R. Acad. Sci. (Paris) II* **1988**, *306* (20), 1423−1425.
(30) Germain, D.; Leocmach, M.; Gibaud, T. *Am. J. Phys.* **2016**, *84* (3), 202−210.
(31) Kurzthaler, C.; Devailly, C.; Arlt, J.; Franosch, T.; Poon, W. C. K.; Martinez, V. A.; Brown, A. T. *Phys. Rev. Lett.* **2018**, *121* (7), 078001.
(32) Mathai, P. P.; Berglund, A. J.; Liddle, J. A.; Shapiro, B. A. *New J. Phys.* **2011**, *13*, 013027.
(33) Takei, H.; Shimizu, N. *Langmuir* **1997**, *13* (7), 1865−1868.
(34) Love, J. C.; Gates, B. D.; Wolfe, D. B.; Paul, K. E.; Whitesides, G. M. *Nano Lett.* **2002**, *2* (8), 891−894.
(35) Hulteen, J. C.; Treichel, D. A.; Smith, M. T.; Duval, M. L.; Jensen, T. R.; Van Duyne, R. P. *J. Phys. Chem. B* **1999**, *103* (19), 3854−3863.
(36) Keane, R. D.; Adrian, R. J. *Appl. Sci. Res.* **1992**, *49* (3), 191−215.
(37) Amendola, V.; Pilot, R.; Frasconi, M.; Marago, O. M.; Iati, M. A. *J. Phys.: Condens. Matter* **2017**, *29* (20), 203002.
(38) Huang, X. H.; Jain, P. K.; El-Sayed, I. H.; El-Sayed, M. A. *Laser Med. Sci.* **2008**, *23* (3), 217−228.
(39) Wang, X.; Baraban, L.; Nguyen, A.; Ge, J.; Misko, V. R.; Tempere, J.; Nori, F.; Formanek, P.; Huang, T.; Cuniberti, G.; Fassbender, J.; Makarov, D. *Small* **2018**, *14* (48), 1803613.
(40) Costagliola, C.; Romano, V.; De Tollis, M.; Aceto, F.; dell'Omo, R.; Romano, M. R.; Pedicino, C.; Semeraro, F. *Mediators Inflammation* **2013**, *2013*, 629529.

https://dx.doi.org/10.1021/acs.analchem.0c01733
Anal. Chem. XXXX, XXX, XXX−XXX